The Ab Initio Melting Curve of Aluminium

Lidunka Vočadlo[1] and Dario Alfè[1,2]
[1]Dept. of Geological Sciences, University College London, Gower Street, London, WC1E 6BT
[2]Dept. of Physics and Astronomy,University College London, Gower Street, London, WC1E 6BT

February 1, 2008

Abstract

The melting curve of aluminium has been determined from 0 to ∼150 GPa using first principles calculations of the free energies of both the solid and liquid. The calculations are based on density functional theory within the generalised gradient approximation using ultrasoft Vanderbilt pseudopotentials. The free energy of the harmonic solid has been calculated within the quasiharmonic approximation using the small-displacement method; the free energy of the liquid and the anharmonic correction to the free energy of the solid have been calculated *via* thermodynamic integration from suitable reference systems, with thermal averages calculated using *ab-initio* molecular dynamics. The resulting melting curve is in good agreement with both static compression measurements and shock data.

1 Introduction

The determination of the melting curves of materials to very high pressures is of fundamental importance to our understanding of the properties of planetary interiors; however, obtaining such melting curves remains a major challenge to experimentalists and theorists alike. In particular, the melting behaviour of iron is of great interest to the Earth science community, since knowledge of this melt transition would help constrain the temperature at the inner core boundary (about 1200 km from the centre of the Earth) which is currently uncertain to within a few thousand degrees. Although several attempts have been made to obtain the melting curve of iron, experimentally and theoretically determined melting curves vary widely with significant disagreement between static compression measurements [1, 2, 3], shock data [4, 5] and first principles calculations [6, 7, 8, 9, 10]. Consequently, the true nature of the melting curve of iron remains in some dispute.

In order to test the reliability of the theoretical techniques used in our previous work on iron and to validate further the reported melting curve [6, 8], we have calculated the melting curve of aluminium, for which there is a plethora of ambient experimental data (e.g. [11]), and for which the experimental melting curve has recently been measured [12, 13, 14].

In the past, a number of theoretical approaches have been used to investigate the melting behaviour of aluminium. Moriarty *et al.* [15] used the generalised pseudopotential theory (GPT) to calculate the free energy of both the solid and liquid. They treated the solid harmonically within the quasiharmonic approximation and for the liquid they used fluid variational theory, where an upper bound for the free energy is calculated from a reference system constructed within GPT. They obtained a melting curve to 200 GPa in fair agreement with more recently determined experiment data [12, 13, 14], predicting a zero pressure melting temperature of 1050K compared to the experimental value of 933K [11]. Mei and Davenport [16] used the embedded atom model (EAM) based on an analytical potential fitted to the structural properties of aluminium. They calculated the free energies of the solid and liquid and obtained

a melting temperature at zero pressure of 800K. Morris *et al.* [17] employed the same EAM model but they used phase coexistence to determine the melting temperature as a function of pressure, with results considerably lower than previous theoretical and experimental estimates; they obtained a zero pressure melting temperature of ∼720 K. Straub *et al.* [18] used first principles calculations to construct an optimal classical potential, and used this potential to calculate the free energies of the solid and the liquid using molecular dynamics; they obtained a zero pressure melting temperature of 955 K.

The first fully *ab-initio* determination of aluminium melting behaviour is that of de Wijs *et al.* [19], who obtained the zero pressure melting point by calculating the free energy of the solid and the liquid entirely from first principles. Their calculations were based on density functional theory (DFT) [20] using the local-density approximation (LDA) for the exchange-correlation energy. The free energy of the solid was obtained as the sum of the free energy of the harmonic solid, within the quasiharmonic approximation, and the full anharmonic contribution, calculated using thermodynamic integration [21] using the harmonic solid as the reference system. For the liquid they used thermodynamic integration with a Lennard-Jones fluid as the reference system. They obtained a melting temperature of 890 K. More recently, Jesson and Madden [22] used the orbital-free (OF) variant of *ab-initio* molecular dynamics and thermodynamic integration to calculate the free energy of liquid and solid aluminium. They found a melting temperature of 615 K, attributing the discrepancy with the DFT-LDA value of de Wijs *et al.* [19] to either the OF approximation or the pseudopotential used.

In this paper we present the first fully *ab-initio* calculations of the entire melting curve of aluminium from 0 to 150 GPa. Our calculations are similar in the general principles to those of de Wijs *et al.* [19] in the sense that we calculate the *ab-initio* free energies of both liquid and solid using thermodynamic integration, although we use the generalised gradient approximation (GGA) [23, 24] for the exchange-correlation energy. In addition to extending the calculations to a wide range of pressures, we also present a more efficient approach to the thermodynamic integration scheme, in which additional intermediate steps are introduced in order to minimise the computational effort. Finally, we discuss some possible limitations of the GGA.

The paper is organised as follows: in section 2 we describe the *ab-initio* simulation techniques and the strategy to calculate the melting curve; in section 3 and 4 we describe the calculations of the free energy of the liquid and the solid respectively, and in section 5 we present the melting properties of aluminium.

2 *Ab-initio* simulation techniques and strategy for melting

In the present work, the aluminium system was represented by a collection of Al^{3+} ions and $3N$ electrons, where N is the number of atoms. The ions were treated as classical particles, and their motion was adiabatically decoupled from that of the electrons *via* the Born-Oppenheimer approximation. For each position of the ions, the electronic problem was solved within the framework of DFT [20] using the GGA of Perdew and Wang [23, 24]. Thermal electronic excitations were included using the standard methods of finite-temperature DFT developed by Mermin [25, 26, 27]. The present calculations were performed with the code VASP [28] which is exceptionally efficient for metals. The interaction between electrons and nuclei was described with the ultrasoft pseudopotential (USPP) method [29]. We used plane-waves with a cut-off of 130 eV. The Brillouin-zone was sampled using Monkhorst-Pack special points [30] (the detailed form of sampling will be noted where appropriate). The extrapolation of the charge density from one step to the next in the *ab-initio* molecular dynamics (AIMD) simulations was performed using the technique described by Alfè [31], which improves the efficiency of the calculations by almost a factor of two. The time step used in our simulations was 1 femto-second.

To calculate the melting temperature we calculated the Gibbs free energy of both the solid and the

liquid as a function of pressure and temperature, $G_s(P,T)$ and $G_l(P,T)$ and, at each chosen P, obtained the melting temperature, T_m, from $G_s(P,T_m) = G_l(P,T_m)$. In fact, we calculated the Helmholtz free energy $F(V,T)$ as a function of volume and temperature, and the Gibbs free energy was obtained from the usual expression $G = F + PV$, where $P = -(\partial F/\partial V)_T$ is the pressure. The main problem in determining melting curves with this technique is the high precision with which the free energies need to be calculated. This is because the Gibbs free energy of the liquid crosses the Gibbs free energy of the solid at a shallow angle, the difference in the slopes being the entropy change on melting. For aluminium this is about 1.4 $k_{\rm B}$/atom at zero pressure, which means that an error of 0.01 eV/atom in either G_s or G_l results in an error of ≈ 80 K in the melting temperature. Therefore, it is important to reduce non-cancelling errors between the liquid and the solid to an absolute minimum. In the next sections we give a detailed discussion of the techniques that we have used to calculate the free energies of the liquid and the solid, and report what the *controllable* errors are: those due to **k**-point sampling, finite size, and statistical sampling. We also try to give an estimate of what the *uncontrollable* errors due to DFT-GGA may be.

3 Free energy of the liquid

The Helmholtz free energy F of a classical system containing N particles is:

$$F = -k_{\rm B}T \ln \left\{ \frac{1}{N!\Lambda^{3N}} \int_V d\mathbf{R}_1 \dots d\mathbf{R}_N \, e^{-\beta U(\mathbf{R}_1,\dots \mathbf{R}_N;T)} \right\}, \tag{1}$$

where $\Lambda = h/(2\pi M k_{\rm B}T)^{1/2}$ is the thermal wavelength, with M the nuclear mass, h the Plank's constant, $k_{\rm B}$ the Boltzmann constant and $\beta = 1/k_{\rm B}T$. The multidimensional integral extends over the total volume of the system V.

A direct calculation of F using the equation above is impossible, since it would involve knowledge of the potential energy $U(\mathbf{R}_1,\dots \mathbf{R}_N;T)$ for all possible positions of the N atoms in the system. We have used instead the technique known as thermodynamic integration [21], as developed in earlier papers [32, 33, 19, 34]. This is a general scheme to compute the free energy difference $F - F_0$ between two systems whose potential energies are U and U_0 respectively. In what follows we will assume that F is the unknown free energy of the *ab-initio* system and F_0 is the known free energy of a reference system. The free energy difference $F - F_0$ is the reversible work done when the potential energy function U_0 is continuously and reversibly switched to U. To do this switching, a continuously variable energy function U_λ is defined such that for $\lambda = 0, U_\lambda = U_0$ and for $\lambda = 1, U_\lambda = U$. We also require U_λ to be differentiable with respect to λ for $0 \le \lambda \le 1$. A convenient form is:

$$U_\lambda = (1 - f(\lambda))U_0 + f(\lambda)U, \tag{2}$$

where $f(\lambda)$ is an arbitrary continuous and differentiable function of λ with the property $f(0) = 0$ and $f(1) = 1$. The Helmholtz free energy of this *hybrid* system is:

$$F_\lambda = -k_{\rm B}T \ln \left\{ \frac{1}{N!\Lambda^{3N}} \int_V d\mathbf{R}_1 \dots d\mathbf{R}_N \, e^{-\beta U_\lambda(\mathbf{R}_1,\dots \mathbf{R}_N;T)} \right\}, \tag{3}$$

Differentiating this with respect to λ gives:

$$\frac{dF_\lambda}{d\lambda} = -k_B T \frac{\frac{1}{N!\Lambda^{3N}} \int_V d\mathbf{R}_1 \dots d\mathbf{R}_N e^{-\beta U_\lambda(\mathbf{R}_1,\dots \mathbf{R}_N;T)} (-\beta \frac{\partial U_\lambda}{\partial \lambda})}{\frac{1}{N!\Lambda^{3N}} \int_V d\mathbf{R}_1 \dots d\mathbf{R}_N e^{-\beta U_\lambda(\mathbf{R}_1,\dots \mathbf{R}_N;T)}} = \left\langle \frac{\partial U_\lambda}{\partial \lambda} \right\rangle_\lambda, \tag{4}$$

so

$$\Delta F = F - F_0 = \int_0^1 d\lambda \left\langle \frac{\partial U_\lambda}{\partial \lambda} \right\rangle_\lambda . \tag{5}$$

For our calculations we defined U_λ thus:

$$U_\lambda = (1-\lambda)\, U_0 + \lambda U. \tag{6}$$

Differentiating U_λ with respect to λ and substituting into Equation 5 yields:

$$\Delta F = \int_0^1 d\lambda \, \langle U - U_0 \rangle_\lambda . \tag{7}$$

Under the ergodicity hypothesis, thermal averages are equivalent to time averages, so we calculated $\langle \cdot \rangle_\lambda$ using AIMD, taking averages over time, with the evolution of the system determined by the potential energy function U_λ. The temperature was controlled using a Nosé thermostat [35, 36]. It is important to stress that the choice of the reference system does not affect the final answer for F, although it does affect the efficiency of the calculations. The latter can be understood by analysing the quantity $\langle U - U_0 \rangle_\lambda$. If this difference has large fluctuations then one would need very long simulations to calculate the average value to a sufficient statistical accuracy. Moreover, for an unwise choice of U_0 the quantity $\langle U - U_0 \rangle_\lambda$ may strongly depend on λ so that one would need a large number of calculations at different λ's in order to compute the integral in Eq. 7 with sufficient accuracy. It is crucial, therefore, to find a good reference system, where "good" means a system for which the fluctuations of $U - U_0$ are as small as possible. In fact, if the fluctuations are small enough, we can simply write $F - F_0 \simeq \langle U - U_0 \rangle_0$, with the average taken in the reference ensemble. If this is not good enough, the next approximation is readily shown to be [7]:

$$F - F_0 \simeq \langle U - U_0 \rangle_0 - \frac{1}{2 k_\mathrm{B} T} \left\langle [U - U_0 - \langle U - U_0 \rangle_0]^2 \right\rangle_0 . \tag{8}$$

This form is particularly convenient since one only needs to sample the phase space with the reference system, and perform a number of *ab-initio* calculations on statistically independent configurations extracted from a long classical simulation.

To evaluate the integral in Equation 7 one can calculate the integrand $\langle U - U_0 \rangle_\lambda$ at a sufficient number of λ and calculate the integral numerically.

Alternatively, one can adopt the dynamical method described by Watanabe and Reinhardt [37]. In this approach the parameter λ depends on time, and is slowly (adiabatically) switched from 0 to 1 during a single simulation. The switching rate has to be slow enough so that the system remains in thermodynamic equilibrium, and adiabatically transforms from the reference to the *ab-initio* system. The change in free energy is then given by:

$$\Delta F = \int_0^{T_\mathrm{sim}} dt \frac{d\lambda}{dt} \left(U - U_0 \right), \tag{9}$$

where T_sim is the total simulation time, $\lambda(t)$ is an arbitrary function of t with the property of being continuous and differentiable for $0 \leq t \leq 1$, $\lambda(0) = 0$ and $\lambda(T_\mathrm{sim}) = 1$.

When using this second method, it is important to ensure that the switching is adiabatic, i.e. that T_sim is sufficiently large. This can be achieved by changing λ from 0 to 1 in the first half of the simulation, and then from 1 back to 0 in the second half of the simulation, evaluating ΔF in each case; the average of the two values is then taken as the best estimate for ΔF, and the difference is a measure of the non-adiabaticty.

If this difference is less than the desired statistical uncertainty, one can be confident that the simulation time is sufficiently long.

In our calculations we chose a total simulation time of sufficient length such that the difference in ΔF between the two calculations was less than a few meV/atom. We return later to estimate the errors in our calculations in Section 3.5.

As pointed out by Jesson and Madden [22], a possible problem in the calculation of the thermodynamic integral is that the system U_λ may be in the solid region of the phase diagram, even though the two end members U_0 and U are in the liquid region. If this happens, the system can freeze during the switching, and the integration path is not reversible, leading to an incorrect result. For small systems the situation is even more problematic, since the phase diagram is not defined by sharp boundaries, and the system can freeze even if it is above the melting temperature of the corresponding system in the thermodynamic limit. We have ourselves experienced freezing of the system for some simulations at temperatures very close to the melting point; in order to avoid including the results from these simulations, we carefully monitored the mean square displacement and the structure factor of the system, and included only those simulations in which these two quantities clearly indicated liquid behaviour throughout the whole simulation.

3.1 The reference system

We mentioned earlier that the efficiency of the calculations is entirely determined by the quality of the reference system, i.e. by the strength of the fluctuations of $\Delta U = U - U_0$. The key to the success of these simulations, therefore, is being able to find a reference system such that the fluctuations in ΔU are as small as possible. Based on the experience of previous work on liquid Al [19] and liquid Fe [6, 8] we experimented with the Lennard-Jones (LJ) system and an inverse power potential (IP). Analysis of the fluctuations in ΔU indicated that the system which best represented the liquid was the IP:

$$U_{\mathrm{IP}} = \frac{1}{2} \sum_{I \neq J} \phi(\mid \mathbf{R}_I - \mathbf{R}_J \mid), \tag{10}$$

where

$$\phi(r) = \frac{B}{r^\alpha}. \tag{11}$$

The potential parameters B and α were chosen by minimising the quantity:

$$\left\langle \left[U_{\mathrm{IP}}\left(B,\alpha\right) - U - \left\langle U_{\mathrm{IP}}\left(B,\alpha\right) - U \right\rangle \right]^2 \right\rangle \tag{12}$$

with respect to B and α, where $\langle\rangle$ means the thermal average in the ensemble generated by the *ab-initio* potential. To investigate whether the optimum values for the potential parameters depended strongly on thermodynamic state, we performed the optimisation at the three thermodynamic states of the extremes of high P/T and low P/T, and also a point in between; we found that the single choice of $B = 246.67$ and $\alpha = 6.7$ (units of eV and Å) was equally good for all states and we therefore used these two parameters for all our calculations.

It may be surprising that such a simple inverse power potential can reproduce the energetics of the liquid with sufficient accuracy, since simple repulsive potentials cannot describe metallic bonding. One may think that a more realistic potential such as those based on the EAM [16, 38, 39, 40] would be more appropriate, since these potentials explicitly contain a repulsive and a bonding term. However, in our recent work on iron [7] we tested the use of an EAM potential as a reference system and found that the bonding term is almost independent of the positions of the atoms, depending only on the volume and temperature of the system, and the fluctuations of the energy are almost entirely due to the repulsive term. Since the only relevance in this work is the strength of the fluctuations (Eq. 12), little is gained by using an EAM rather then a much simpler inverse power potential.

3.2 Free energy of the reference system

Consider the excess free energy of the IP, $F_{\rm IP}^{\rm ex} = F_{\rm IP} - F_{\rm PG}$, where $F_{\rm PG}$ is the Helmholtz free energy of the perfect gas and $F_{\rm IP}$ the total Helmholtz free energy of the IP system. The very simple functional form of $U_{\rm IP}$ makes it easy to show that the adimensional quantity $F_{\rm IP}^{\rm ex}/k_{\rm B}T$ can only depend non-trivially on a single thermodynamic variable, rather then separately on V and T:

$$F_{\rm IP}^{\rm ex}/k_{\rm B}T = f(\zeta) \tag{13}$$

with

$$\zeta = B/V^{\alpha/3}k_{\rm B}T. \tag{14}$$

The free energy of the IP has been studied extensively in the past [41], but only for special values of the exponent α, which did not include our own $\alpha = 6.7$. We have therefore explicitly calculated the free energy of our inverse power potential using thermodynamic integration as before, but this time we started from a system of known free energy, the Lennard-Jones liquid, whose potential function is given by

$$U_{\rm LJ} = 4\varepsilon\left[\left(\frac{\sigma}{r}\right)^{12} - \left(\frac{\sigma}{r}\right)^{6}\right]. \tag{15}$$

The free energy of the Lennard-Jones liquid, $F_{\rm LJ}$, has been accurately tabulated by Johnson *et al.* [42]. To calculate $F_{\rm IP} - F_{\rm LJ} = \Delta F_{\rm LJ\to IP}$ we used simulation cells containing 512 atoms with periodic boundary conditions and a simulation time $T_{\rm sim} = 200$ ps. We performed the calculations for ζ ranging from 2.5 to 6.25, with steps of 0.25. The calculations were done at a fixed volume of 14 Å^3/atom and varing temperatures according to Equation 14. We carefully checked that the results were converged to better than 1 meV/atom with respect to the size of the simulation cell and the length of the simulations. To avoid truncating the inverse power potential at a finite distance we used the Ewald technique. Our results were fitted to a third order polynomial in ζ:

$$f(\zeta) = \sum_{i=0}^{3} c_i \zeta^i. \tag{16}$$

The coefficients are: $c_0 = 2.4333; c_1 = 27.805; c_2 = -5.0704; c_3 = 1.5177$, and the fitting function reproduced the calculated data such that the errors in $F_{\rm IP}$ were generally less than 1 meV per atom.

As an additional check on the calculated free energy, we repeated most of the simulations using the perfect gas as the reference system, thereby avoiding the inclusion of any possible errors that may exist in the free energy of the LJ system reported in the literature [42]. For these calculations we used a different form for U_λ, namely:

$$U_\lambda = \lambda^2 U_{\rm IP} \tag{17}$$

(the potential energy of the perfect gas is zero, so does not appear in the formula). So Eq. 5 becomes

$$F_{\rm IP} - F_{\rm PG} = \int_0^1 d\lambda\, 2\lambda \langle U_{IP}\rangle_\lambda. \tag{18}$$

The advantage of using this different functional form for U_λ is that the value of the integrand does not need to be computed for $\lambda = 0$, where the dynamics of the system is determined by the perfect gas potential. In this case, since there are no forces in the system there is nothing stopping the atoms from overlapping, and the potential energy $U_{\rm IP}$ diverges. Not computing the integrand at $\lambda = 0$ partially solves this problem, but for small values of λ where the forces on the atoms are small, the atoms can come close together and the potential energy, $U_{\rm IP}$, fluctuates violently. However, we found that by performing long enough simulations, typically 1 ns, we could calculate the integral with an accuracy of ≈ 1 meV/atom, and, within the statistical accuracy, we found the same results as those obtained using the LJ reference system.

3.3 Free energy of the *ab-initio* system

To calculate the full *ab-initio* free energy of the liquid, $F_{\rm liq}$, we used thermodynamic integration, starting from the IP system. The calculations were performed at 18 different thermodynamic states over a range of volumes (9.5-19.5 Å^3/atom) and temperatures (800-6000 K). To address the issue of **k**-point sampling and cell size errors in the free energy difference $F_{\rm liq} - F_{\rm IP}$, tests were carried out on cells containing up to 512 atoms and a $5 \times 5 \times 5$ **k**-point grid (calculations on the largest 512 atoms cell were only performed with Γ-point sampling), at $V = 16.5$ and $T = 1000K$. The free energy difference $F_{\rm liq} - F_{\rm IP}$ was calculated using the perturbational approach (Eq. 8), with sets of configurations generated using the IP potential. We found that a 64-atom cell with a $3 \times 3 \times 3$ **k**-point grid was sufficient to get convergence to within 2 meV/atom. However, we were reluctant to perform simulations using the desired $3 \times 3 \times 3$ **k**-point grid (14 points in the Brillouin Zone (BZ)) since these calculations are extremely expensive. We found it more efficient to add one further step to our thermodynamic integration scheme:

$$\Delta F_{\Gamma \rightarrow 333} = F_{333} - F_{\Gamma} = \int_1^0 d\lambda \left\langle U_{333} - U_{\Gamma} \right\rangle_{\lambda} , \tag{19}$$

where U_{333} and U_{Γ} are the *ab-initio* total energies calculated using the $3 \times 3 \times 3$ **k**-point grid and Γ-point sampling respectively, and F_{333} and F_{Γ} are the corresponding free energies. To evaluate the free energy difference $\Delta F_{\Gamma \rightarrow 333}$ we noticed that the difference $U_{333} - U_{\Gamma}$ did not depend significantly on the position of the atoms, so the integral in Eq. 19 could be evaluated using the second order formula (Eq. 8). Using a long Γ-point *ab-initio* simulation, we extracted up to 25 statistically independent configurations and calculated the *ab-initio* energies using the $3 \times 3 \times 3$ **k**-point grid. To test this, we performed spot checks at two thermodynamic states, where we calculated the full thermodynamic integral $F_{333} - F_{\rm IP}$ using adiabatic switching with a switching time of ≈ 2 ps, and found the same results to within a few meV/atom.

The free energy difference $\Delta F_{\rm IP \rightarrow \Gamma} = F_{\Gamma} - F_{\rm IP}$ was obtained by full thermodynamic integration between the *ab initio* and reference system using adiabatic switching (Eq. 9) with a switching time of 5 ps, which resulted in errors of 1(4) meV/atom in the low(high) P/T region. To test this, we also calculated this free energy difference at several state points by numerical evaluation of the thermodynamic integral (Eq. 5), with $\lambda = 0$, 0.5 and 1; we found that this gave the same numerical answer to within our statistical errors.

In summary, the free energy of the liquid was obtained from a series of thermodynamic integration calculations:

$$F_{\rm liq} = F_{333} = F_{\rm LJ} + \Delta F_{\rm LJ \rightarrow IP} + \Delta F_{\rm IP \rightarrow \Gamma} + \Delta F_{\Gamma \rightarrow 333}. \tag{20}$$

3.4 Representation of the free energy of the liquid

The results of the calculations described in the previous section were fitted to a suitable function of T and V. In order to do that efficiently we expressed the free energy in the following way:

$$F_{\rm liq} = F_{\rm IP} + \Delta F = F_{\rm IP} + \Delta U^s + (\Delta F - \Delta U^s) \tag{21}$$

where $\Delta U^s = U^s - U^s_{\rm IP}$, with U^s the zero temperature ab-initio (free) energy of the face-centred-crystal (fcc) and $U^s_{\rm IP}$ the inverse power energy. U^s can be calculated very accurately, details of which will be given below in Section 4.1; $U^s_{\rm IP}$ has no errors. The remaining quantity $\Delta F - \Delta U^s$ is a weak function of V and T, and was fitted to a polynomial in V and T:

$$\Delta F - \Delta U^s = \sum_{j=0}^{1} \left(\sum_{i=0}^{3} a_{ij} V^i \right) T^j \tag{22}$$

The fitting reproduced the calculated data to within ≈ 2 meV/atom.

3.5 Error estimates for $F_{\rm liq}$

The errors on $F_{\rm IP}$ and ΔU^s are each less than 1 meV/atom (see Section 4.1 below). The part of the free energy that carries the largest errors is $\Delta F - \Delta U^s$, which we estimate to be 2(5) meV/atom at low(high) P/T.

4 Free energy of the solid

The free energy of the solid can be represented as the sum of two contributions: the free energy of the perfect non-vibrating fcc crystal and that arising from atomic vibrations above zero Kelvin:

$$F_{\rm sol} = F_{\rm perf} + F_{\rm vib}. \tag{23}$$

The contribution to the free energy due to the vibrations of the atoms may be written:

$$F_{\rm vib} = F_{\rm harm} + F_{\rm anharm} \tag{24}$$

where $F_{\rm harm}$ is the free energy of the high temperature crystal in the harmonic approximation and $F_{\rm anharm}$ is the anharmonic contribution.

4.1 Free energy of the perfect crystal

The free energy of the perfect crystal, $F_{\rm perf}$, was calculated as a function of volume and temperature. Calculations were performed on a fcc cell at a series of volumes (9.5-19.5 Å^3/atom representing compression up to $\sim$ 150 GPa) and temperatures (up to 6000K) with a 24x24x24 **k**-point grid (equivalent to 1300 points in the irreducible wedge of the Brilloiun zone (IBZ)), which ensures convergence of the (free) energies to better than 1 meV/atom. At each different temperature we calculated the *ab-initio* (free) energy as a function of volume, and then performed a least-square fit of the results to a third-order Birch-Murnaghan equation of state:

$$E(V) = E_0 + \frac{3}{2}V_0K\left[\frac{3}{4}(1+2\xi)\left(\frac{V_0}{V}\right)^{4/3} - \frac{\xi}{2}\left(\frac{V_0}{V}\right)^{2} - \frac{3}{2}(1+\xi)\left(\frac{V_0}{V}\right)^{2/3} + \frac{1}{2}\left(\xi+\frac{3}{2}\right)\right] \tag{25}$$
$$\xi = \frac{3}{4}(4-K').$$

The parameters E_0, V_0, K_0, and K' were fitted to a fourth order polynomial as function of temperature:

$$E_0(T) = \sum_{i=0}^{4} e_{0,i}T^i; \qquad V_0(T) = \sum_{i=0}^{4} v_{0,i}T^i; \qquad K_0(T) = \sum_{i=0}^{4} k_{0,i}T^i; \qquad K'(T) = \sum_{i=0}^{4} k'_{0,i}T^i. \tag{26}$$

The fitting reproduced the calculated energies to better than 1 meV/atom in the whole P/T range.

4.2 Free energy of the harmonic crystal

The free energy of the harmonic crystal is given by:

$$F_{\rm harm}(V,T) = -\left(\frac{3k_{\rm B}T}{\Omega_{\rm BZ}N_i}\right)\sum_i \int_{\rm BZ}\left(\ln\left[\frac{k_BT}{\hbar\omega_{\mathbf{q},i}(V,T)}\right] - \frac{1}{24}\left[\frac{\hbar\omega_{\mathbf{q},i}(V,T)}{k_{\rm B}T}\right]^2 + \ldots\right)d\mathbf{q} \tag{27}$$

where $\omega_{\mathbf{q},i}(V,T)$ are the phonon frequencies of branch i and wavevector $\mathbf{q}$, $\Omega_{\rm BZ}$ is the volume of the Brillouin zone, N_i is the total number of phonon branches and the dependence on temperature of $\omega_{\mathbf{q},i}$ is due to electronic excitations. We truncate the summation after the first term, which is the classical limit of the free energy:

$$F_{\rm harm} = -\left(\frac{3k_{\rm B}T}{\Omega_{\rm BZ}N_i}\right)\sum_i \int_{\rm BZ}\left(\ln\frac{k_{\rm B}T}{\hbar\omega_{\mathbf{q},i}}\right)d\mathbf{q}. \tag{28}$$

This is a justifiable approximation to make for two reasons: (i) the error in making such a truncation is very small (<1 meV/atom), and (ii) neglecting the higher order terms, i.e., the quantum corrections, is consistent with the liquid calculations where the motions of the atoms were treated classically.

It is useful to express the harmonic free energy in terms of the geometric average $\bar{\omega}$ of the phonon frequencies, defined as:

$$\ln\bar{\omega} = \frac{1}{N_{\mathbf{q}}N_i}\sum_{\mathbf{q},i}\ln(\omega_{\mathbf{q}i}), \tag{29}$$

where we have replaced the integral $\frac{1}{\Omega_{\rm BZ}}\int_{\rm BZ} d\mathbf{q}$ with the summation $\frac{1}{N_{\mathbf{q}}}\sum_{\mathbf{q}}$. This allows us to write:

$$F_{\rm harm} = 3k_{\rm B}T\ln(\beta\hbar\bar{\omega}). \tag{30}$$

To calculate the vibrational frequencies $\omega_{\mathbf{q},i}$, we used our own implementation [43] of the small displacement method [44, 7].

The central quantity in the calculation of the phonon frequencies is the force-constant matrix $\Phi_{is\alpha,jt\beta}$, since the frequencies at wavevector $\mathbf{q}$ are the eigenvalues of the dynamical matrix $D_{s\alpha,t\beta}$, defined as:

$$D_{s\alpha,t\beta}(\mathbf{q}) = \frac{1}{\sqrt{M_sM_t}}\sum_i \Phi_{is\alpha,jt\beta}\exp\left[i\mathbf{q}\cdot(\mathbf{R}_j^0+\tau_t-\mathbf{R}_i^0-\tau_s)\right]\ . \tag{31}$$

where $\mathbf{R}_i^0$ is a vector of the lattice connecting different primitive cells, τ_s is the position of the atom s in the primitive cell and M_s its mass. If we have the complete force-constant matrix, then $D_{s\alpha,t\beta}$, and hence the frequencies $\omega_{{\rm q}l}$, can be obtained at any $\mathbf{q}$. In principle, the elements of $\Phi_{is\alpha,jt\beta}$ are non-zero for arbitrarily large separations $\mid \mathbf{R}_j^0+\tau_t-\mathbf{R}_i^0-\tau_s \mid$, but in practice they decay rapidly with separation, so a key issue in achieving our target precision is the cut-off distance beyond which the elements can be neglected.

In the harmonic approximation the α Cartesian component of the force exerted on the atom at position $\mathbf{R}_i^0+\tau_s$ is given by:

$$F_{is\alpha} = -\sum_{jt\beta}\Phi_{is\alpha,jt\beta}\ u_{jt\beta} \tag{32}$$

where $u_{js\beta}$ is the displacement of the atom in $\mathbf{R}_j^0+\tau_t$ along the direction β. The force constant matrix can be calculated *via*:

$$\Phi_{is\alpha,jt\beta} = -\frac{F_{is\alpha,jt\beta}}{u_{jt\beta}} \tag{33}$$

where all the atoms of the lattice are displaced one at a time along the three Cartesian components by $u_{jt\beta}$, and the forces $F_{is\alpha,jt\beta}$ induced on the atoms in $\mathbf{R}_i^0+\tau_s$ are calculated. Since the crystal is invariant under translations of any lattice vector, it is only necessary to displace the atoms in one primitive cell and calculate the forces induced on all the other atoms of the crystal, so that we can simply put $j=0$. The fcc crystal has only one atom in the primitive cell, so only three displacements are needed. However, a displacement along the x direction is equivalent by symmetry to a displacement along the y or the z

direction, and therefore only one displacement along an arbitrary direction is needed. It is convenient to displace the atom along a direction of high symmetry, so that the supercell has the maximum possible number of symmetry operations. These can be used to reduce the number of **k**-points in the IBZ, minimising the computational effort. For an fcc crystal this is achieved by displacing the atom along the diagonal of the cube.

Tests for cell-size (64-512 atoms), displacement length (0.01-0.0005 fraction of nearest neighbours distance) and **k**-point grid (up to $9 \times 9 \times 9$) were performed at the two extremes of high P/T and low P/T state points. Convergence of the free energy to within less than 3 meV/atom was achieved using a 64-atom cell with a 0.001 fractional displacement and a $9 \times 9 \times 9$ k-point grid (equivalent to 85 points in the IBZ of the supercell). Calculations were performed for $V = 9.5 - 18.5$ Å^3 and $T = 500 - 6000K$, and $\ln(\bar{\omega})$ has been fitted to the following polynomial in V and T:

$$\ln(\bar{\omega}) = \sum_{j=0}^{3} \left(\sum_{i=0}^{3} a_{ij} V^i \right) T^j. \tag{34}$$

The fitting reproduced the calculated data within ≈ 1 meV/atom.

4.3 Anharmonicity

To obtain the anharmonic contribution to the free energy of the solid we have again used thermodynamic integration. In this case a natural choice for the reference system could be the harmonic solid [19], but unfortunately this does not reproduce the *ab initio* anharmonic system with sufficient accuracy. A much better reference system is a linear combination of the harmonic *ab-initio* and the same IP used for the liquid calculations [7]:

$$U_{\rm ref} = aU_{\rm IP} + bU_{\rm harm}, \tag{35}$$

where the harmonic potential energy is:

$$U_{\rm harm} = \frac{1}{2} \sum_{is\alpha, jt\beta} u_{is\alpha} \Phi_{is\alpha, jt\beta}\ u_{jt\beta}, \tag{36}$$

and where $u_{js\beta}$ is the displacement of the atom in $\mathbf{R}_j^0 + \tau_t$ along the direction β, and $\Phi_{is\alpha,jt\beta}$ is the force constant matrix. The parameters a and b are determined by minimising the fluctuations in the energy differences $U_{\rm ref} - U$ on a set of statistically independent configurations generated with $U_{\rm ref}$. However, when we start our optimisation procedure we do not know $U_{\rm ref}$, so we cannot use it to generate the configurations. We could use the *ab-initio* potential, but this would involve very expensive calculations. We used instead an iterative procedure, like in our previous work on iron [7]. We generated a set of configurations using the harmonic potential $U_{\rm harm}$ and calculated the *ab-initio* energies. By minimising the fluctuations of $U_{\rm ref} - U$ we found a first estimate for a and b, and we constructed a first estimate of $U_{\rm ref}$. We generated a second set of configurations using this $U_{\rm ref}$, calculated the *ab-initio* energies and minimised again the fluctuations of $U_{\rm ref} - U$ with respect to a and b. This procedure could be continued until the values of a and b no longer changed, but in practice we stopped after the second step, and found $a = 0.95$ and $b = 0.12$. We did not use the extra freedom in the choice of the inverse power parameters since we found that this reference system already described the energetics of the solid very accurately.

The calculation of the anharmonic part of the free energy required, once more, two thermodynamic integration steps. In the first step we calculated the free energy difference $F_{\rm ref} - F_{\rm harm}$. These are cheap calculations since they involve only the classical potentials $U_{\rm IP}$ and $U_{\rm harm}$; the simulations were performed with cells containing 512 atoms for 10 ps, which ensured convergence of the free energy difference

$F_{\rm ref}-F_{\rm harm}$ to within 1 meV/atom. In the second step we calculated $F_{\rm vib}-F_{\rm ref}$ where, since the fluctuations in the energy differences $U-U_{\rm ref}$ were very small, we were able to use the second order formula (Eq. 8).

The problem in the calculation of thermal averages for a nearly harmonic system is that of ergodicity. For an harmonic system different degrees of freedom do not exchange energy, so in a system which is close to being harmonic the exploration of phase space using molecular dynamics can be a very slow process. We solved this problem following Ref. [19] whereby the statistical sampling was performed using Andersen molecular dynamics [45], in which the atomic velocities are periodically randomised by drawing them from a Maxwellian distribution. This type of simulation generates the canonical ensemble and overcomes the ergodicity problem.

All the calculations were performed on a 64-atom cell with kpoints in a $7\times7\times7$ grid for the high P/T state points and a $9\times9\times9$ grid for the low P/T state points equivalent to 172 or 365 points in the IBZ respectively.

The anharmonic contribution to the free energy of the solid turns out to be very small, being positive and equal to only a few meV/atom at low pressure and approximatively -20 meV/atom at high pressure.

4.4 Error estimates for $F_{\rm sol}$

The errors in $F_{\rm perf}$ are less than 1 meV/atom, the errors in $F_{\rm harm}$ are $\approx$ 3(4) meV/atom at low(high) P/T and the errors in $F_{\rm ahnarm}$ are $\approx$ 1(4) meV/atom at low(high) P/T; the total errors in $F_{\rm sol}$ are $\approx$ 3(6) meV/atom at low(high) P/T.

5 Results and discussion

We display in Figure 1 our calculated melting curve compared with the experimental zero pressure value [11], the DAC high pressure results [12, 13] and the high pressure shock datum [14]. We also report in Figures 2a, 2b and 2c the volume change on melting, V_m, the entropy change on melting, S_m, and the melting gradient, dT_m/dP, respectively. The errors in the melting curve arise from the errors in the calculated free energies and are $\approx$ 50(100) K in the low(high) pressure part of the diagram respectively.

The overall agreement with the experiments is extremely good; however, the low pressure results differ by more than 15 % (at zero pressure, 786 K compared with the experimental value of 933 K). Indeed, at zero pressure the agreement between the calculated and experimental volume change on melting and dT_m/dP is rather poor (see Table 1). In addition, our calculations are not in very good agreement with the previous calculations of de Wijs *et al.* [19], although this is not necessarily surprising, since these latter calculations were based on LDA, while ours are based on GGA. Nevertheless, one might expect the results from LDA and GGA to be similar, since Al is a nearly free-electron like metal and therefore one would expect a very good DFT description with both LDA and GGA. To explore a possible reason why GGA does not predict the melting properties of aluminium very accurately we consider the zero pressure crystal equilibrium volume. This is predicted by GGA to be $\approx$ 2% larger than the experimental value; this means that the calculated pressure for the experimental zero pressure volume is $\approx$ +1.6 GPa. To see how this error propagates in melting properties we may devise a correction to the Helmholtz free energy such that the pressure is rectified:

$$F_{\rm corr} = F + \delta PV, \tag{37}$$

with $\delta P = 1.6$ GPa. Using $F_{\rm corr}$ in our calculations we found the *corrected* melting curve, represented by the dotted line in Fig. 1, where we assumed δP to be the same in the whole P/T range. The zero pressure corrected melting temperature is 912 K, which is in very good agreement with the experimental value 933 K. The corrected volume change on melting, entropy change on melting and dT_m/dP are also in much

better agreement with the experimental numbers. The correction is less important at high pressure, where dT_m/dP is smaller.

This point may be further illustrated by looking at the zero pressure phonon dispersion curves for Al. Since phonon frequencies depend on the interatomic forces, their correctness is surely important in the context of melting. In Figure 3 we display the GGA calculated phonon dispersion curves compared with experimental data [46]. Our calculations were performed both at the GGA zero pressure equilibrium volume and the experimental volume (both at 80 K). We notice that the agreement is good (though not perfect) if the calculations are performed at the experimental volume, and rather poor if the calculated zero pressure GGA volume is used instead. This indicates that GGA will probably yield better results if the GGA pressure is corrected in order to match the experimental data.

In their work, de Wijs *et al.* [19] found good agreement between LDA and experiments. In their case a *corrected* LDA would lower the zero pressure melting point below 800 K. In order to understand this apparent different behaviour between LDA and GGA we have also calculated the phonons using LDA at the calculated equilibrium volume and also at the experimental volume (both at 80K). These are also reported in Fig. 3. In accord with previous LDA calculations [47] we found very good agreement with the experiments when the phonons are calculated at the LDA zero pressure volume, but the agreement becomes poor at the experimental volume, which is consistent with the result for the melting temperature [19].

In conclusion, both GGA and LDA predict an incorrect equilibrium volume at a fixed pressure, although LDA yields very good results for both the phonon dispersion curves and the zero pressure melting properties (which is probably accidental). For GGA the incorrect equilibrium volume propagates to an incorrect description of the phonon frequencies and the melting properties. If the GGA pressures are corrected so as to match the experimental data, the phonon dispersion and the melting properties come out in very good agreement with the experiments. These two behaviours are internally consistent, but point to an intrinsic error due to the use of GGA. Quantum Monte-Carlo (QMC) techniques [48] have been shown to predict the energetics with much higher accuracy than DFT [49], and calculations for systems containing more than 100 atoms have already been reported [50]. We believe that in the near future it will be possible to use QMC for more accurate calculations of free energies.

To summarise, we have calculated the melting curve of aluminium entirely from first-principles within the DFT-GGA framework. Our work is based on the calculation of the Gibbs free energy of liquid and solid Al, and for each fixed pressure the melting temperature is determined by the point at which the two free energies cross. Our results are in good agreement with the available experimental data, although they reveal an intrinsic DFT-GGA error which is responsible for an error of ≈ 150K in the low pressure melting curve. This error is probably due to the incorrectly predicted pressure by GGA, and it becomes less important in the high pressure region, as dT_m/dP becomes smaller.

Acknowledgements

We both acknowledge the support of Royal Society University Research Fellowships; we also thank Mike Gillan and John Brodholt for useful discussions. LV thanks Humphrey Vocadlo for his assistance during the course of this research.

References

[1] Q. Williams, R. Jeanloz, J. D. Bass, B. Svendesen, T. J. Ahrens, Science **286**, 181 (1987).

[2] R. Boehler, Nature **363**, 534 (1993).

[3] G. Shen, H. Mao, R. J. Hemley, T. S. Duffy and M. L. Rivers, Geophys. Res. Lett. **25**, 373 (1998).

[4] J. M. Brown and R. G. McQueen, J. Geophys. Res. **91**, 7485 (1986).

[5] C. S. Yoo, N. C. Holmes, M. Ross, D. J. Webb and C. Pike, Phys. Rev. Lett. **70**, 3931 (1993).

[6] D. Alfè, M. J. Gillan and G. D. Price, Nature **401**, 462 (1999).

[7] D. Alfè, G. D. Price, M. J. Gillan, Phys. Rev. B, in press.

[8] D. Alfè, G. D. Price, M. J. Gillan, unpublished.

[9] A. Laio, S. Bernard, G. L. Chiarotti, S. Scandolo and E. Tosatti, Science **287**, 1027 (2000).

[10] A. B. Belonoshko, R. Ahuja, and B. Johansson, Phys. Rev. Lett. **84**, 3638 (2000).

[11] *CRC Handbook of Chemistry and Physics*, Editor D. R. Lide, New York, 77th edition (1996-1997).

[12] R. Boehler, M. Ross, Earth Planet. Sci. Lett. **153**, 223 (1997)

[13] A. Hänström, P. Lazor, J. of Alloys and Compounds **305**, 209 (2000).

[14] J. W. Shaner, J. M. Brown, R. G. McQueen, in High pressure in Science and Technology. Editors C. Homan, R. K. Mac Crone, E. Whalley, North Holland, Amsterdam, 137 (1984).

[15] J. A. Moriarty, D. A. Young, and M. Ross, Phys. Rev. B **30**, 578 (1984).

[16] J. Mei, J. W. Davenport, Phys. Rev. B **46**, 21 (1992).

[17] J. R. Morris, C. Z. Wang, K. M. Ho, and C. T. Chan, Phys. Rev. B **49**, 3109 (1994).

[18] G. K. Straub, J. B. Aidun, J. M. Willis, C. R. Sanchez-Castro, and D. C. Wallace, Phys. Rev. B **50**, 5055 (1994).

[19] G. A. de Wijs, G. Kresse and M. J. Gillan, Phys. Rev. B **57**, 8223 (1998).

[20] P. Hohenberg and W. Kohn, Phys. Rev. **136**, B864 (1964); W. Kohn and L. Sham, Phys. Rev. **140**, A1133 (1965); R. O. Jones and O. Gunnarsson, Rev. Mod. Phys. **61**, 689 (1989); M. J. Gillan, Contemp. Phys. **38**, 115 (1997).

[21] For a discussion of thermodynamic integration see e.g. D. Frenkel and B. Smit, *Understanding Molecular Simulation*, Academic Press, San Diego (1996).

[22] B. J. Jesson and P. A. Madden, J. of Chem. Phy. **113** 5924 (2000).

[23] Y. Wang and J. Perdew, Phys. Rev. B **44**, 13298 (1991).

[24] J. P. Perdew, J. A. Chevary, S. H. Vosko, K. A. Jackson, M. R. Pederson, D. J. Singh and C. Fiolhais, Phys. Rev. B **46**, 6671 (1992).

[25] N. D. Mermin, Phys. Rev. **137**, A1441 (1965).

[26] M. J. Gillan, J. Phys. Condens. Matter **1**, 689 (1989).

[27] R. M. Wentzcovitch, J. L. Martins and P. B. Allen, Phys. Rev. B **45**, 11372 (1992).

[28] G. Kresse and J. Furthmüller, Phys. Rev. B **54**, 11169 (1996); a discussion of the ultra-soft pseudopotentials used in the VASP code is given in G. Kresse and J. Hafner, J. Phys. Condens. Matter **6**, 8245 (1994).

[29] D. Vanderbilt, Phys. Rev. B **41**, 7892 (1990).

[30] H. J. Monkhorst and J. D. Pack, Phys. Rev. B **13**, 5188 (1976).

[31] D. Alfè, Comp. Phys. Commun. **118**, 31 (1999).

[32] O. Sugino and R. Car, Phys. Rev. Lett. **74**, 1823 (1995).

[33] E. Smargiassi, P. A. Madden, Phys Rev B **51**, 117 (1995).

[34] D. Alfè, G. A. de Wijs, G. Kresse and M. J. Gillan, Int. J. Quant. Chem. **77**, 871 (2000).

[35] S. Nosé, Molec. Phys., **52** 255 (1984); J. Chem. Phys. **81**, 511 (1984).

[36] F. D. Di Tolla and M. Ronchetti, Phys. Rev. B **48**, 1726 (1993).

[37] M. Watanabe and W. P. Reinhardt, Phys. Rev. Lett. **65**, 3301 (1990).

[38] M. S. Daw, S. M. Foiles, and M. I. Baskes, Mat. Sci. Rep. **9**, 251 (1993).

[39] M. I. Baskes, Phys. Rev. B **46**, 2727 (1992).

[40] A. B. Belonoshko, and R. Ahuja, Phys. Earth Planet. Inter. **102**, 171 (1997).

[41] B. B. Laird and A. D. J. Haymet, Mol. Phys. **75**, 71 (1992).

[42] K. Johnson, J. A. Zollweg, and E. Gubbins, Mol. Phy. **78**, 591 (1993).

[43] Program available at `http://chianti.geol.ucl.ac.uk/dario`

[44] G. Kresse, J. Furthmüller and J. Hafner, Europhys. Lett. **32** 729 (1995).

[45] H. C. Andersen, J. Chem. Phys. **72**, 2384 (1980).

[46] R. Stedman, and G. Nilsson, Phys. Rev. **145**, 492 (1966).

[47] S. de Gironcoli, Phys. Rev. B. **51**, 6773 (1995)

[48] B. L. Hammond, W. A. Lester, Jr., & P. J. Reynolds, *Monte Carlo Methods in Ab Initio Quantum Chemistry*, World Scientific, Singapore, (1994).

[49] G. Rajagopal, R. J. Needs, A. James, S. D. Kenny, & W. M. C. Foulkes, Phys. Rev. B **51**, 10591 (1995).

[50] P. R. C. Kent, R. Q. Hood, A. J. Williamson, R. J. Needs, W. M. C Foulkes, G. & Rajagopal, Phys. Rev. B **59**, 1917 (1999).

[51] J. F. Cannon, J. Phys. Chem. Ref. Data 3, 781 (1974).

[52] M. W. Chase, Jr., C. A. Davies, J. R. Downey, Jr., D. J. Frurip, R. A. McDonald and A. N. Syverud, J. Phys. Chem. Ref. Data Suppl. 14, 1 (1985).

	Experiment	LDA	GGA	GGA - corrected
T_m (K)	933	890 (20)	786 (50)	912 (50)
S_m (k_B)	1.38	1.36 (4)	1.35 (6)	1.37 (6)
V_m (Å^3)	1.24	1.26 (20)	1.51 (10)	1.35 (10)
dT_m/dP (K GPa^{-1})	65	67 (12)	81	71

Table 1: Comparison of *ab initio* and experimental melting properties of Al at zero pressure. Values are given for the melting temperature, T_m, entropy change on melting, S_m, volume change on melting, V_m, and melting gradient dT_m/dP. The LDA results are from Ref. [19]; the experimental values for T_m, S_m and dT_m/dP are from Refs. [11], [52] and [51] respectively, and the experimental melting volume, V_m, is calculated using the Clapeyron relation, $V_m = S_m dT_m/dP$.

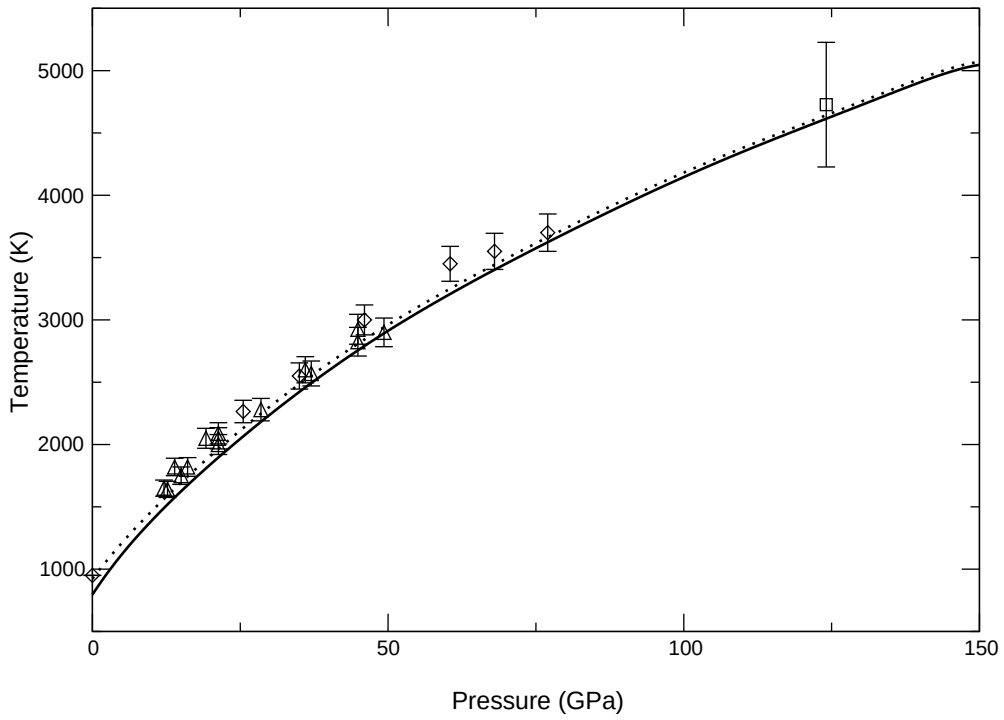

Figure 1: Comparison of melting curve of Al from present calculations with previous experimental results. Solid curve: present work; dotted curve: present work with pressure correction (see text); diamonds and triangles: DAC measurements of Refs. [12] and [13] respectively; square: shock experiments of Ref. [14].

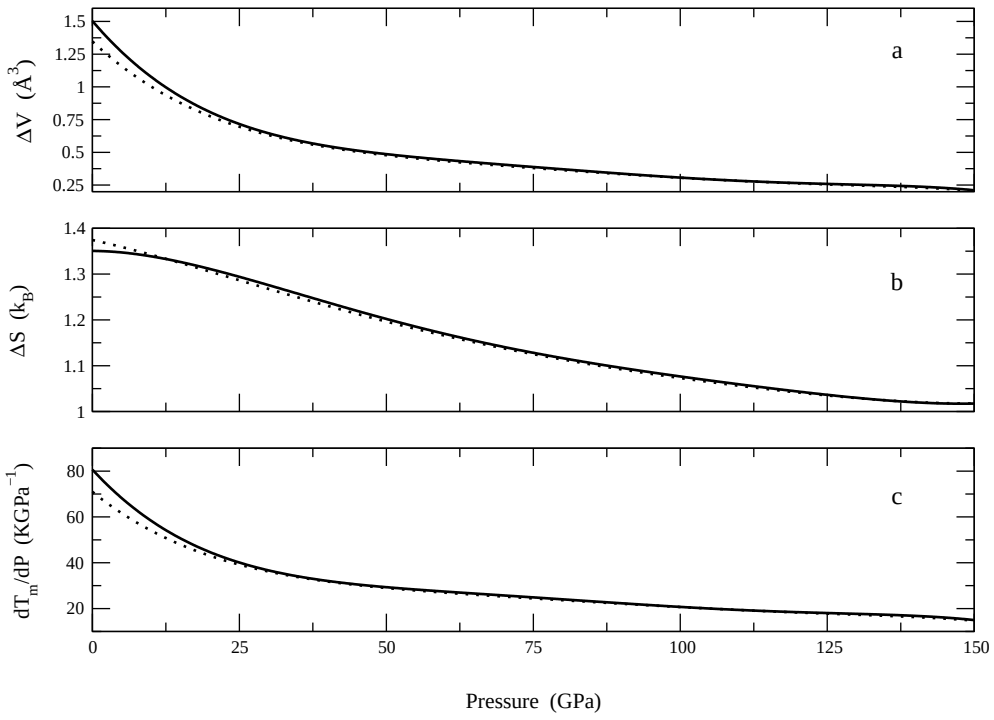

Figure 2: Calculated pressure dependence of the melting properties of Al: a) volume change on melting, b) entropy change on melting and c) melting gradient. Solid curve: present work; dotted curve: present work with pressure correction (see text).

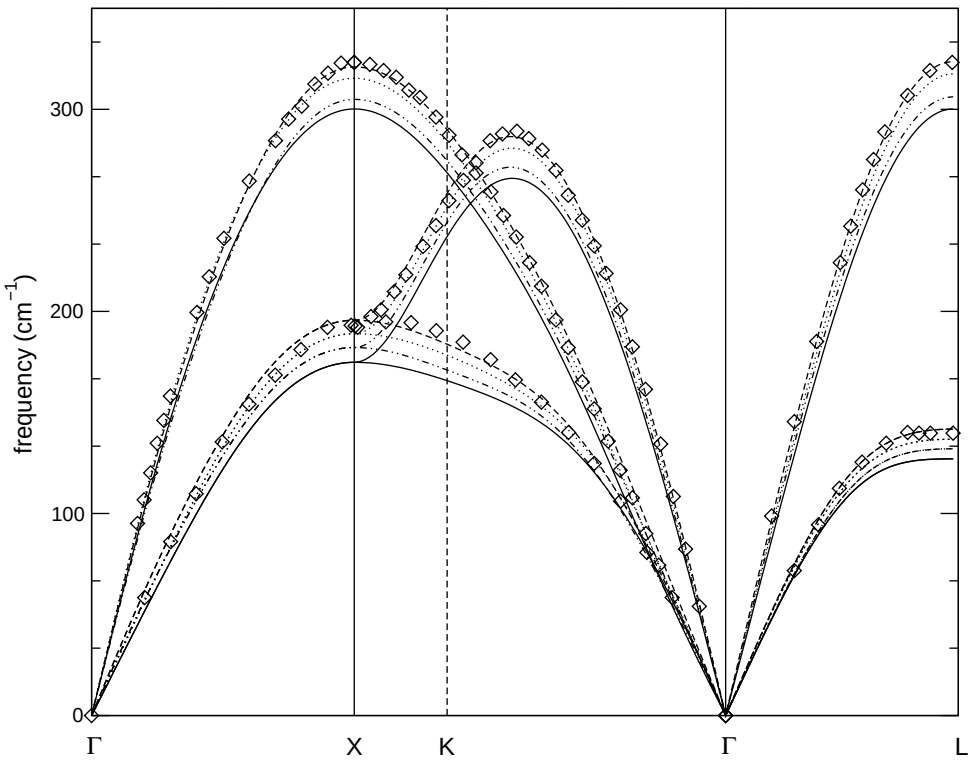

Figure 3: Comparison of the phonon dispersion curve for Al from present calculations with previous experimental results. Solid curves: present work with GGA; dotted curves: present work with GGA and with pressure correction (see text); dashed curves: present work with LDA; dot-dashed curves: present work with LDA and with pressure correction (see text); diamonds: experiments from Ref. [46].